1.0

1.1

1.25

4.5
5.0
5.6

2.8
3.2
3.6
4.0

2.5
2.2
2.0
1.8

1.4

1.6

MICROCOPY RESOLUTION TEST CHART
NATIONAL BUREAU OF STANDARDS-1963-A

ADA038835

(12)

DEVELOPMENT AND AERODYNAMICS OF
PROBOSCIOID ABLATING NOSE TIPS

R. Vaglio Laurin

March 1977

D D C

RECEIVED

APR 29 1977

B

FINAL SCIENTIFIC REPORT

NEW YORK UNIVERSITY

FACULTY OF ARTS AND SCIENCE
DEPARTMENT OF APPLIED SCIENCE

DEVELOPMENT AND AERODYNAMICS OF PROBOSCIOID ABLATING NOSE TIPS

ABSTRACT

Rationalization of slender concave shapes on ablating nose tips is
obtained in terms of composite laminar/turbulent self-preserving
solutions to the nose recession problem. The occurrence of sub-
critical and critical (violently oscillatory) flow conditions is
discussed and associated with specific geometrical characteristics
of the ablating nose shape. The presence of distinct oscillatory
modes is noted for both the subcritical and critical cases, and the
distinct underlying inviscid instability mechanisms are pointed out.
On that basis numerical flow analyses by extension of available
unsteady inviscid flow models is suggested, and the nature of the
required extensions is outlined.

I. INTRODUCTION

Recent laboratory and flight experiments have exhibited large departures between predicted (Refers. 1 and 2) and observed (Ref. 3) equilibrium shapes for ablating nose tips, such as are used on high performance ballistic reentry vehicles. Since reliable estimates of nose tip configuration and survival are essential to the determination of vehicle aerodynamics, the divergence between theory and experiments must be resolved and improved predictive methods of ablative shape change need be developed with attention to the novel aspects of flow field behavior (e.g., violent oscillations) revealed in the experiments.

A two step approach to the problem has been followed in the investigations reported here. A qualitative theoretical rationalization of the observed shapes has been sought first. Upon resolution of this matter, the dynamics of the associated flow fields have been examined and the formulation of relevant numerical models has been extracted. The first phase has largely depended upon theoretical considerations based on approximate analytical models. By contrast, the second phase has largely relied on data analyses.

The lines of inquiry followed in the two phases of the research and the related results are presented sequentially in the main body of the report. First, rationalization of the slender concave configurations observed in the experiments is obtained on the basis of self-preserving (equilibrium) solutions to the nose recession problem under conditions where transition from laminar to turbulent flow regime occurs on the nose (Section II). Upon the determination of equilibrium solutions which exhibit the desired geometrical characteristics, wind tunnel data for typical configurations of interest are examined with specific attention to the presence of oscillations

and the nature of the underlying instability mechanisms (Section III). In this process the association of subcritical and critical (violently oscillatory) flow situations with specific geometrical characteristics of the ablating nose shape is established. The development of either family of shapes as a function of transition Reynolds number vis a vis flight Reynolds number is discussed. The essentially inviscid nature of the instability mechanisms underlying the oscillations is pointed out. Based upon this last determination requirements for the numerical analysis of the considered flow fields are set forth; extensions of available unsteady inviscid flow techniques meeting those requirements are outlined (Section IV).

II. SELF PRESERVING ABLATING NOSE TIPS

Whereas previous theoretical studies of equilibrium (self-preserving)
nose shapes,in either strictly laminar (Ref. 1) or turbulent (Ref. 2)
flow,identified only blunt configurations, the experiments of Reference 3
have shown that relatively slender concave shapes also develop within particu-
lar ranges of Reynolds.number. In fact, two classes of such shapes arise
(Figure 1): the first,sometimes designated as sub-critical turbulent, is
characterized by relative overall slenderness, and steady, either attached
or separated, boundary layer around the concave portion of the nose; the second,
sometimes designated as critical turbulent, is characterized by relative over-
all bluntness,separated boundary layer around the concave portion of the
nose, unsteady shock layer and random nose tip asymmetries.

An examination of the data readily reveals a distinction between the viscous
flow regimes encountered in the experiments (Ref. 3) and assumed in the
analyses (Refs. 1 and 2). In the experiments, transition from laminar to
turbulent regime probably occurs near the beginning of the concave portion
of the nose; in the analyses a single viscous flow regime is considered. Thus,
a resolution of the problem is suggested in terms of matched, spatially
sequenced,nose contour portions, respectively described by laminar and tur-
bulent self-preserving solutions. The possibility is analyzed below. For
that purpose the existence of self preserving laminar and turbulent solutions
consistent with concave nose shapes is examined first. The matching of a
laminar and a turbulent solution,to yield configurations of the type shown
in Figure 1,is then considered.

-3-

With a view to obtaining closed form results the analysis is carried
out under several simplifying assumptions, namely: . 1) perfect gas
flow with hypersonic free stream velocity; 2) pressure distribution on the
body described by Newtonian theory; 3) boundary layer flow attached to
the body and amenable to representation by local similarity solutions;
4) uniform wall enthalpy and effective heat of ablation per unit volume
of the surface material. These approximations, almost classical in studies
of viscous hypersonic flows, and specifically used in References 1 and 2,
generally yield results of sufficient accuracy for purposes of problem defi-
nition, as addressed here. With the notation of Figure 1 for coordinate sys-
tem and body geometry, the local laminar (q_ℓ) and turbulent (q_t, flat plate
reference enthalpy) heat transfer rates are then given by (Refs. 4 and 2).

$$\dot{q}_\ell = 0.33 \ Pr^{-2/3} \ (H_e - H_w)(p_e/p_o)(U_e/U_\infty)r^j \left[\frac{\rho_o \ \mu_o \ U_\infty}{\int_o^s (p_e/p_o)(U_e/U_\infty)r^{2j}ds} \right]^{1/2} \tag{1}$$

$$\dot{q}_t = 0.03 \ Pr^{-2/3} \ (H_e - H_w) \ (\rho_r \ U_e \ s/\mu_r)^{0.8}(\mu_r/s) \tag{2}$$

where H, p, U, ρ, μ, Pr respectively denote stagnation enthalpy, pressure,
velocity, density, viscosity, Prandtl number, subscripts ℓ, t respectively
identify laminar and turbulent flow situations, subscripts e, w, r, o respec-
tively characterize flow properties at the edge of the boundary layer, at the
wall, at an intermediate reference condition, and at the stagnation point.
Pressure and velocity distributions at the edge of the boundary layer
are described by

$$(P_e/P_o \ ) = \cos^2\theta \tag{3a}$$

$$(U_e /U_\infty) = [1 - (\cos\theta)^{2(\gamma-i)/\gamma}]^{1/2} \tag{3b}$$

for blunt configurations, and by

-4-

$$(p_e/p_o) = \cos^2\theta \qquad\qquad\qquad (4a)$$

$$(U_e/U_\infty) = 1 + 0(\cos^2\theta) \qquad\qquad\qquad (4b)$$

for slender configurations.

Self-preserving shapes are determined by solutions of the equation

$$(\dot{q}/\cos\theta) = \dot{x}\, H_{eff} = \text{constant} \qquad\qquad\qquad (5)$$

with $\dot{q}$ described by either equation (1) or (2) in conjunction with either (3a,b) or (4a,b).

Substitution of (1) into (5) yields the following equation for the self preserving laminar nose shape.

$$C_\ell r^{2j}\, f^2(\theta) = \int_o^r f(\theta)\, r^{2j}\, dr \qquad\qquad\qquad (6)$$

where C_ℓ is the constant

$$C_\ell = 0.33\ Pr^{-2/3}\,(H_e - H_w)\rho_0\mu_0 U_\infty \ (\cos\theta/\dot{q}_\ell) \qquad\qquad\qquad (7a)$$

and

$$f(\theta) = (p_e/p_o)(U_e/U_\infty)\,(\cos\theta)^{-1} \qquad\qquad\qquad (7b)$$

a function rendered explicit by (3a,b) and (4a,b).

The solution is

$$r = 2(j + 1)\, C_\ell f(\theta) \qquad\qquad\qquad (8a)$$

complemented by the geometrical relation

$$\dot{x} = \int_o^r \tan\theta\ dr \qquad\qquad\qquad (8b)$$

Upon substitution of (3a,b) and (7b) into (8a,b) the blunt self preserving laminar shape is obtained, viz.

-5-

$$r = R_N \left(\frac{\gamma}{\gamma-1}\right)^{\frac{1}{2}} \cos\theta [1-(\cos\theta)^{2(\gamma-i)/\gamma}]^{\frac{1}{2}} \tag{9a}$$

$$x = R_N \left(\frac{\gamma}{\gamma-1}\right)^{\frac{1}{2}} \{\sin\theta \, [1 - (\cos\theta)^{2(\gamma-i)/\gamma}]^{\frac{1}{2}}$$
$$- \int_0^\theta (\cos\theta)^{-1}[1-(\cos\theta)^{2(\gamma-i)/\gamma}]^{\frac{1}{2}}ds\} \tag{9b}$$

where

$$R_N = 2(\dot{j} + 1) \left(\frac{\gamma-1}{\gamma}\right)^{\frac{1}{2}} \dot{C}_\ell (\rho_0 \mu_0 U_\infty)^{-1} \tag{10}$$

is the (arbitrary) radius of curvature of the nose at the stagnation point,
inversely proportional to the square of the recession rate ($\dot{q}_\ell/\cos\theta \, H_{eff}$).
The magnitude of R_N and of the recession rate become uniquely defined
only upon stipulation of the value $\theta = \theta_s$ at the nose shoulder. In that
connection it is noted that the blunt self-preserving shape (9a,b) exhibits
a maximum in r for

$$\theta = \theta_\ell = \cos^{-1} \left(\frac{\gamma}{2\gamma-1}\right)^{\gamma/2(\gamma-1)} \tag{11}$$

e.g., $\theta_\ell = 49.9°$ for $\gamma = 7/5$. With attention restricted to values $\theta_s \leq \theta_\ell$,
the magnitude of the radius of curvature R_N (the recession rate $\dot{q}_\ell/\cos\theta \, H_{eff}$)
is minimized (maximized) by the choice $\theta_s = \theta_\ell$. An alternate choice (Refs. 1
and 2) is to set $\theta_s = \theta^*$, θ^* being the body inclination at the sonic point
defined by the assumed Newtonian pressure distribution (3e), viz.

$$\theta^* = \cos^{-1}[2/(\gamma + 1)]^{\gamma/2(\gamma - 1)} \tag{12}$$

which satisfies the condition $\theta^* < \theta_\ell$ for $1 \leq \gamma \leq 2$. For $\gamma = 7/5$ the
two assumptions, either $\theta_s = \theta_\ell$ or $\theta_s = \theta^*$, lead essentially to the
self-preserving shape as shown in Figure 2.

The quest for slender self-preserving laminar shapes, defined by equations
(4a, b) (7b) and (8a,b), proves to be fruitless because logarithmically

-6-

divergent values of x are obtained as $r \to o$ and $\theta = \cos^{-1}r \to (\pi/2)$.

Substitution of (2) into (5) readily yields an algebraic relation between s and θ for a self preserving turbulent shape, viz.

$$s = C_t(\mu_r/\mu_0)[(T_0/T_r)(P_e/P_0)(U_e/U_\infty)]^4 (\cos\theta)^{-5}$$

where C_t is the constant

$$C_t = [0.03 \, Pr^{-2/3}(H_e - H_w)\mu_0(\cos\theta/\dot{q}_t)]^5 [\rho_0 U_\infty/\mu_0]^4 \qquad (13)$$

With the further reasonable assumption $T_r = T_0$ the turbulent self-preserving shape is described by

$$s = C_t[(p_e/p_0)(U_e/U_\infty)]^4 (\cos\theta)^{-5} \qquad (14a)$$

Complemented by the geometrical relations

$$r = \int_0^s \cos\theta \, ds \qquad (14b)$$

$$x = \int_0^s \sin\theta \, ds \qquad (14c)$$

Upon substitution of (3 a,b) and (4a, b) into (14a, b, c), the blunt self-preserving turbulent shape ($\theta \to o$ as $s \to o$)

$$s = C_t (\cos\theta)^3 [1 - (\cos\theta)^{2(\gamma-1)/\gamma}]^2 \qquad (15a)$$

$$r = C_t \left\{ (\cos\theta)^4 [1 - (\cos\theta)^{2(\gamma-1)/\gamma}]^2 - \right.$$

$$(\cos\theta)^4 \left[\frac{1}{4} - \frac{5\gamma - 4}{3\gamma - 1} [\cos\theta]^{2(\gamma-1)/\gamma} + \frac{9\gamma - 8}{8\gamma - 4} (\cos\theta)^{4(\gamma-1)/\gamma}\right] +$$

$$\left. \left[\frac{1}{4} - \frac{5\gamma - 4}{3\gamma - 1} + \frac{9\gamma - 8}{8\gamma - 4}\right]\right\} \qquad (15b)$$

$$x = C_t \left\{ \sin\theta (\cos\theta)^3 [1 - (\cos\theta)^{2(\gamma-1)/\gamma}]^2 - \right.$$

$$\left. \int_0^\theta (\cos\theta)^4 [1 - (\cos\theta)^{2(\gamma-1)/\gamma}]^2 \, d\theta \right\} \qquad (15c)$$

-7-

and the slender self-preserving turbulent shape ($\theta \to \pi/2$ as $s \to o$)

$$s = C_t (\cos \theta)^3 \tag{16a}$$

$$r = (3/4) C_t (\cos\theta)^4 \tag{16b}$$

$$x = (3/16)C_t \{ \sin\theta[4 (\cos\theta)^3 - 2 \cos\theta] + \pi - 2\theta\} \tag{16c}$$

are obtained, respectively. The results (15,a,b,c) are displayed in Figure 3 for $\gamma = 7/5$, while the results (16a,b,c) are shown in Figure 4 for a general γ. The blunt solution is only applicable in the range $0 \lesssim \theta \lesssim \theta_t$ because $(ds/d\theta)$ becomes null at

$$\theta_t = \cos^{-1} \left[\frac{\gamma + 2}{7\gamma - 4}\right]^{\gamma/2(\gamma-1)}$$

e.g. $\theta_t = 55.36°$ for $\gamma = 7/5$. By contrast, the slender solution is applicable to the entire range $(\pi/2) \gtrsim \theta \gtrsim 0$. As in the laminar case, the magnitude of C_t (which has the dimensions of a length)and of the recession rate remain arbitrary until the value $\theta = \theta_s$ at the nose shoulder is specified. For the blunt shape the magnitude of C_t (the recession rate $\dot{q}_t/\cos\theta\, H_{eff}$) is minimized (maximized) by the choice $\theta_s = \theta_t$; for the slender shape the extrema are provided by the choice $\theta_s = 0$.

Whereas the blunt self-preserving laminar and turbulent shapes described by equations (9a,b) and (15a, a, c) essentially coincide with those reported in References 1 and 2, the slender turbulent shape of equations (16a,b,c) represents a novel result which permits rationalization of the experimentally observed sub-critical turbulent shapes. Inspection of Figures 1, 2 and 4, with attention to the indicated location of transition, suggests that the shapes of interest result from the combination of a blunt laminar solution descriptive of the nose tip region together with a slender turbulent solution descriptive of the concave contour region. The assumption of sudden laminar-turbulent transition permits direct joining of the two solutions.

-8-

The requirement of equal recession rate at the joining point, together
with the plausible assumption that the turbulent boundary layer has
negligible thickness (i.e., $\theta = \pi/2$) at that point, readily provide the rela-
tion between the length scales R_N and C_t of the two solutions, viz.

$$C_t/R_N = \{\frac{0.03}{0.33} \; [4(j + 1) \; (\gamma - 1)/\gamma]^{-1/4}\}^5 \; (\frac{\rho_0 U_\infty R_N}{\mu_0})^{1.5}$$

$$= \{\frac{0.03}{0.33} \; [4(j + 1)^2(\gamma - 1)/\gamma]^{-1/4}\}^5 \; [(R_N/s_t) \; Re_t]^{1.5}$$

(17)

in terms of the conventionally defined transition Reynolds number
$Re_t = (\rho_0 U_\infty s_t/\mu_0)$ based on arc length s_t to the joining point. Slight
generalizations of (17) arise with different estimates of the turbulent
boundary layer thickness, or equivalently the value of θ for the slender tur-
bulent shape, at the joining point. In all cases, however, the geometry of the
overall configuration becomes controlled by the magnitude of the transition
Reynolds number Re_t, which sets the length scale ratio C_t/R_N [see equation
(17)]. An example of the transition Reynolds number influence upon nose
geometry is vividly displayed in Figure 5; the family of combined blunt
laminar/slender turbulent solutions is characterized by the following joining
point conditions: $\theta = \theta_\ell$ on the laminar side, $\theta = \pi/2$ on the turbulent side,
parametrically varying magnitude of Re_t. It may be noted that configurations
of increasing overall slenderness are obtained as Re_t increases. Yet one
length scale (either C_t or R_N), and the recession rate, remain undertermined
(as was the case for the fully laminar and fully turbulent solutions) until
the value of $\theta \geq 0$ is prescribed at the station where the overall nose
joins with the afterbody.

The straightforward requirement that the nose cap the given afterbody plays
the rather unexpected role of defining the Reynolds number range over which
combined blunt laminar/slender turbulent solutions can exist. As equations

-9-

(9a) and (16b) show, the ordinate of the nose/afterbody functions is at best

$$(r_s/R_N) = [r(\theta_\ell)/R_N] + (3/4)(C_t/R_N)$$

or

$$r_s = \{[r(\theta_\ell)/s(\theta_\ell)] + (3/4)(C_t/R_N)[R_N/s(\theta_\ell)]\}\frac{Re_t}{(U_\infty/\nu_0)} \tag{18a}$$

Once Re_t is given, the right hand side of (18a) and, therefore, the nose diameter are uniquely determined. The value of r_s so defined must equal or exceed the radius of the afterbody; otherwise, the combined laminar/turbulent solution cannot exist. In view of (18a) the range of Reynolds numbers $Re_s = (U_\infty r_s/\nu_0)$ over which the requirement is satisfied depends on Re_t according to

$$\left[\frac{r(\theta_\ell)}{s(\theta_\ell)}\right] Re_t \leq Re_s \leq \left\{\frac{r(\theta_\ell)}{s(\theta_\ell)} + 3/4\left(\frac{C_t}{R_N}\right)\left[\frac{R_N}{s(\theta_\ell)}\right]\right\} Re_t \tag{18b}$$

The magnitudes of lower (say Re_{s1}) and upper (say Re_{s2}) bounds in (18b) depend on j, γ and Re_t by way of equations (9a,b) and (17); typical values, for $j = 1$, $\gamma = (7/5)$ and selected values of Re_t, are tabulated below

Re_t	Re_{s1}	Re_{s2}	$r_s/r(\theta_\ell)$
10^4	$.921 \times 10^4$	3.252×10^4	3.531
5×10^4	4.605×10^4	1.349×10^6	29.30
10^5	$.921 \times 10^5$	7.462×10^6	81.03
5×10^5	4.605×10^5	4.125×10^8	895.8
10^6	$.921 \times 10^6$	2.332×10^9	2532.0

The calculated values of $r_s/r(\theta_\ell)$ become extremely large for $Re_t \geq 5 \times 10^4$, suggesting that development of the associated blunt-laminar/slender-turbulent configurations may be prevented in practice by reasons of nose tip structural integrity. One may conjecture that the blunt-turbulent solution of Figure 3 would develop under those conditions.

-10-

This view is in qualitative agreement with the experiments of Reference 3, where development of slender concave shapes was observed only over a range of unit Reynolds numbers whose lower and upper bounds differed by a factor less than two.

To summarize, the considerations of this section rationalize the development of slender concave shapes on ablating nose tips. However, they do not explain the different flow behaviors observed with subcritical turbulent and critical turbulent configurations. The presence of unsteady shock layers in the latter case readily suggests that the key to the problem cannot be found in a weak viscous-inviscid intersection viewpoint, as adopted in this section; instead, strong interactions must be allowed for. The broader approach is discussed in the following section.

III. UNSTEADY STRONG INTERACTIONS ON ABLATING NOSE TIPS

Oscillatory shock wave motions,such as are exhibited by the critical
turbulent shapes, have been observed by several investigators working
with ablating bodies (Reference 3), non-ablating spiked and concave conic
bodies (References, 5, 6 7, 8) as well as effectively concave conic bod-
ies as are encountered, for example, with massive lateral injection on
slender cones (Reference 9). The typical qualitative sequence of events
in such oscillatory flows is illustrated in the sketches of Figure 6, which
are based on selected shadowgraphs for the M_∞ = 6.8 flow around a flat-
headed cylinder with a nose spike having length equal to three quarters of
the body diameters (Ref. 5). The cycle starts with the boundary layer on
the spike separating near the nose and forming an approximately conical
dead air region, which, if continued to the face of the body, would strike
it well below the shoulder (Figure 6a). As the separated layer reattaches
on the body non-tangentially, a shock arises at the reattachment point to
turn the supersonic flow just outside the layer up the nose of the body.
Depending upon the magnitude of the angle β (Figure 7) that the separated
layer makes with the tangent to the body at the point of impingement, the
shock is either weak or strong. In the latter case the shock stands off
from the point of impingement, and the flow behind it is subsonic. Inter-
estingly enough, the onset of oscillatory flow is observed only under
these conditions (Reference 5).

The presence of a detached shock and locally subsonic flow at reattachment
has a significant implication in diagnosing the mechanism of the oscillatory
motion. Not only must the mass flow balance be preserved in the dead air
region, as emphasized by previous investigators (Refs. 5,6,7), but also

-12-

the choking requirement at the body shoulder must be satisfied by the external inviscid flow. The recognition of this dual requirement distinguishes the present analysis from those of the previous investigators.

The flow patterns sketched in Figure 7 clearly indicate that the geometry of, and the pressure ratio across, the detached shock are controlled by the details of the reattachment process. The pressure ratio seeks a magnitude such that the mass of air reversed at reattachment balances the mass of air scavenged by the sheer layer. However, the process ignores the choking requirement at the shoulder. Analysis of Figure 6a shows that the attached shock lies closer to the shoulder than would be the case in the steady flow over a flat-headed cylinder without the spike (Reference 10). Under these conditions the mass flow cannot be accomodated through the sonic section; a disturbance must then propagate forward from that section to cause a reduction in mass flow and a simultaneous outward displacement of the detached shock. To be sure the forward propagating disturbance increases the amount of air reversed at reattachment with consequent bulging of the dead air region and the associated bow shock (Figures 6b, c); this process, however, constitutes a concomitant effect rather than the forcing cause of the oscillation. The view is supported by the following discussion of experimental results obtained in Reference 8 with the blunt PANT-1 nose configuration and the relatively slender proboscioid (1-10-10) configuration (Figure 8) at $M_\infty = 3.0$.

The flow over the PANT-1 configuration exhibits a catostrophic oscillation with reduced frequency (Strouhal number) $S = (fD/U_\infty) \approx 0.227$. As the separated free shear layer has a time-averaged inclination of 37° relative to the axis (Figure 9), the flow deflection at reattachment exceeds the maximum allowable for the prevailing Mach number. A strong reattachment shock

-13-

develops, which, in the course of the oscillation, moves between most
forward and most rearward loci almost parallel to each other (Figure 9). The
back-and-forth motion covers the relatively small distance of 0.2 D, less than
the estimated detachment distance of 0.27D (measured from the shoulder) for
an 80° half-angle cone. The time averaged shock location (identified as
Pitot shock in Figure 9) is consistent with that estimated for steady M_∞ = 3.0
flow over the 80° half angle cone. The time averaged pressure distribution over
the portion of the nose included between the average reattachment point and the
shoulder also agrees with the same steady flow estimate. Thus, the time-aver-
aged results are independent of the detailed mechanism of bubble growth and
collapse. Instead, an unsteady choking process is indicated as underlying
the oscillation.

The choking instability viewpoint is further supported by the particular magni-
tude of the reduced frequency S. The associated period $\tau = f^{-1}_c$ (4.4D/U_∞) =
(D/0.23U_∞) is approximately equal to twice the average transit time of a fluid
element across the inviscid hypersonic flow over the nose; thus, the shock oscilla-
tion is geared with the oscillations in size of, and mass flow through, the
sonic station. In line with the transit time scaling under hypersonic condi-
tions (viz M $\gtrsim$ 3 for the blunt configurations considered here) the period of
oscillation, when present, is insensitive to details of the nose shape and to
the magnitude of the free stream Mach number and Reynolds number (References
5,6,7 and 8). However, the geometry and flow parameters influence the sta-
bility boundaries for the oscillation (Refs. 5 and 7). In brief, the shape and
size of the dead air region are controlled by the flow at the reattachment
point. The very low velocities in the region endow it with a fast response
time. Accordingly, the shear layer tends to move so that standard separation
relations (e.g. Reference 6 for laminar flow situations and Reference 11 for
turbulent flow situations) as well as the Chapman reattachment condition are

-14-

satisfied. The strong reattachment shock generated in this process violates the choking requirement, and wave disturbances ensue in the inviscid portion of the flow. The waves upset the equilibrium in the dead air region and cause it to rapidly respond by swelling (shrinking) as flow reversal at the reattachment point increases (decreases). The sequence of events depicted in Figure 6 for a spiked body then follows. As air flows into it, the recirculation region begins to enlarge causing a nearly normal shock at the spike tip (Fig. 6b) to replace the initial conical shock wave (Fig. 6a). The shock wave grows from the spike tip as more air is fed into the recirculation region which assumes a blunt shape (Figure 6c). The associated shock pattern resembles that produced by a jet of air from the body injected against the main stream (Fig. 6f). Simultaneously , the mass flow through the shoulder throat decreases and the reattachment point moves up the face of the body. As the choking requirement is accommodated, the disturbance from the sonic station changes sign causing air to be drained from the recirculation region. The region then begins to collapse and the shock wave, which was at the spike tip, moves toward the body (Fig. 6d). In the process separation again occurs at the spike tip with a conical shock formed (Fig. 6e). When the strong shock returns sufficiently close to the body (as in Fig. 6a) the cycle begins again.

The question as to whether the oscillation is due to unsteady choking or an inherent inviscid instability of the mean flow profiles upstream of the strong shock remains to be examined. High frequency oscillations have been observed in experiments and calculations for the flow field around the proboscioid (1-10-10) configuration (Fig. 8, Refs. 8 and 12) at widely different Reynolds numbers($5 \times 10^4 \leq Re_D \leq 1.5 \times 10^5$ in the experiments of Reference 8 versus $Re_D = 4.6 \times 10^3$ in the calculations of Reference 12),different free stream Mach numbers ($M_\infty = 3$ in the experiments and $M_\infty = 10$ in the calculations) and in the presence of quite different flow patterns (separated flow in the

-15-

experiments versus attached flow in the calculations). These oscillations, however, are quite distinct from those observed with the PANT-1 configuration. The reduced frequencies $S = (fD/U_\infty)$ are quite large ($4.5 \lesssim S \lesssim 9$ for the experiments and $S \approx 8.2$ for the calculated fundamental frequency); shock wave motions, if present at all, are quite modest (Fig. 10). Measurable fluctuations are confined to the portion of the inviscid flow where body and shock wave converge to provide a channelling effect and, therefore, spatial amplification. Oscillations with the noted characteristics cannot be associated with a choking instability because: a) the reattachment shock is weak so that no sonic section arises downstream of it; b) the periods of oscillation are smaller than the average transit time of a fluid element across the inviscid flow region where measurable oscillations prevail (Fig. 10). In view of the modest sensitivity of the reduced frequency to Reynolds number, the driving mechanism must then reside in an inviscid instability connected with the presence of an inflection point in the streamwise velocity profiles over the concave portion of the nose. Such an inflection clearly exists in the separated flows encountered in the experiments; its presence in the attached flow of the calculation has been pointed out in Reference 12. Interestingly enough, the inflection point and the oscillation disappear if calculations are carried out in the inviscid limit (Ref. 12).

To summarize, oscillations can be expected in flows around subcritical turbulent as well as supercritical turbulent ablating nose shapes. The former are associated with relatively slender configuration where the attachment of the separated flow, if present, is accompanied by a weak shock; the latter are associated with blunt configurations, where separation always arises and reattachment is accompanied by a strong detached shock. In all cases, viscous flow processes provide the qualitative flow pattern features which lead to

-16-

instability, viz. inflected velocity profiles in subcritical situations and strong reattachment shocks in critical situations. However, driving and or amplifying mechanisms for the oscillation are of an inviscid nature. Thus, analysis of the flows in question requires a strong interaction coupling of viscous and inviscid flow regions; however, without resort to extremely careful description of the transport processes. In view of the complex flow fields involved, the analysis is necessarily numerical in nature. An outline of a relevant approach is presented in the following section.

In connection with applications to flight vehicles it must be noted that the solution of the oscillatory flow field problem does not avoid the operational difficulties associated with their occurrence. The key resides in nose tip material selection. In fact, the results of Section II indicate that development of slender concave shapes is most probable in flows characterized by a low transition Reynolds number, i.e., flows over nose-tips whose materials develop critical roughness upon ablation. According to Figure 5 the lower the transition Reynolds number the blunter the shape which can be expected at a given flight Reynolds number (based on afterbody diameter) and, therefore, the more likely the onset of critical regime. Conversely, for fixed transition Reynolds number and afterbody size, evolution of the nose toward a blunter shape and a critical regime can be expected as the unit Reynolds number increases. A first cut determination of material's adequacy in avoiding onset of critical conditions, for given trajectory and initial nose configuration/size, can probably be carried out by means of simplified heat transfer analyses (such as those of Section II) in conjunction with available transient ablation codes.

IV. COMMENTS ON NUMERICAL FLOW FIELD MODELS

The discussion of Section III as to the inviscid nature of the oscillation mechanism under subcritical and critical conditions bears directly on the selection of numerical models descriptive of the considered flows. As pointed out in the discussion, the numerical model must realistically describe inflections in streamwise velocity profiles in the subcritical case, and formation of strong unsteady reattachment shock waves in the critical case. At first sight, these features seem to require use of a viscous flow model, i.e., the numerical integration of Navier Stokes equations. However, the brute force approach proves to be impractical even with the most advanced computer facilities because: a) the flows of interest are characterized by high Reynolds numbers and, therefore, by confinement of important viscous transports within regions having thickness much smaller than the typical nose dimension; b) fully three-dimensional unsteady flows must be considered, as distinct azimuthal modulations of the oscillation arise, at least in the critical case (Ref. 8). Thus, the Navier-Stokes attack would entail a four dimensional problem over a domain which involves an inordinately large number of mesh points. For these reasons the study of Reference 12 was restricted to axisymmetric situations and low Reynolds numbers; the associated attached flow field may not exhibit the interaction leading to the critical oscillation.

The viewpoint of this report is that extensions of available inviscid flow models (e.g., Refs. 13 and 14) provide the key to a realistic solution of the problem. The required flow field features due to viscous processes and interactions are embodied in the calculation by introducing the separating

-18-

boundary layer as a source of vorticity, which is convected along the boundary of the recirculation region and drained, consistent with mass conservation considerations, by a singularity located at the point of reattachment. Within this framework transports are neglected within the recirculation region. The overall structure of the flow pattern is attributed to the inviscid interaction between the recirculating flow and the external flow, which includes the strongly rotational portion originating from the separated boundary layer. This portion, which retains the required features of inflectional velocity profiles in the sub-critical case and interactive shock formation in the critical case, can be resolved with a reasonable mesh size, particularly in the important region of reattachment where the lateral scale of of the strongly vortical flow is enhanced by the large local adverse pressure gradients.. Empirical justification for the view resides in the past, reasonably successful, use of the model for studies of steady near wake flows past slender two-dimensional bodies.

-19-

V. CONCLUDING REMARKS

The development and aerodynamics of slender concave configurations
on ablating nose tips have been analyzed. Rationalization of these
shapes has been obtained in terms of novel self-preserving (equilibrium)
solutions of the nose recession problem in the presence of transition
from laminar to turbulent flow regime on the nose. Based upon a study
of these solutions and their domains of existence, the development of
subcritical and critical configurations has been associated with the
relative magnitudes of the transition Reynolds number (based on wetted
length to transition) and the flight Reynold number (based on body
frustrum diameter). In that connection an important role of surface
material and its roughness has been noted.

Upon a reexamination of available experimental data the distinction
between subcritical and critical conditions has been associated with
the geometrical characteristics of the nose shape; specifically, critical
behaviour (i.e. large shock and flow field oscillations) arises only with
blunt configurations characterized by boundary layer separation near the
tip followed by reattachment on nose portions which require strong re-
attachment shocks. The presence of distinct oscillatory modes has been
noted for the subcritical and critical cases, and the distinct underlying
inviscid instability mechanisms have been pointed out. On that basis
the adequacy of numerical analysis by extension of available inviscid flow
field models has been suggested, and the nature of the required extensions
has been outlined.

REFERENCES

1. Hains, F.D., "Equilibrium Shape of an Ablating Nose in Laminar Hypersonic Flow". AIAA J., Vol. 8, No. 7, July 1970, pp. 1354-1355

2. Welsh, W.E., Jr., "Shape and Surface Roughness Effects on Turbulent Nosetip Ablation". AIAA J., Vol. 8, No. 11, Nov. 1970, pp. 1983-1989.

3. Abbett, M. J., Cooper, L., Dahm, T.J. and Jackson, M.D., "Unsteady Flow on Ablated Nose-Tip Shape·, PANT Series G Test and Analysis Report", Aerotherm Rept. 73-87, Acurex Corp., Dec., 1973.

4. Dorrance, W.D., "Viscous Hypersonic Flow", McGraw-Hill Book Co., New York, 1962.

5. Maull, D.J., "Hypersonic Flow over Axially Symmetric Spiked Bodies", Jour. Fluid Mech., Vol. 8, No. 4, 1960, pp. 584-592.

6. Wood, C.J., "Hypersonic Flow over Spiked Cones", Jour. Fluid Mech., Vol. 12, No. 4, 1964, pp. 614-624

7. Abbett, M.J., Cooper, L., Dahm, T.J. and Jackson, M.D., "Flow Characteristics About Concave Conic Forebodies at $M_\infty = 5$"., AIAA J., Vol. 13, No. 11, Nov. 1975, pp. 1419-1420.

8. Demetriades, A. and Laderman, A.J., "Advanced Penetration Problems Program Final Report, Volume I". SAMSO TR No. 75-51, Dec. 1974.

9. Rosenbaum, H., Siegelman, D. and Boger, R.C., "Flowfield Interactions Induced by Massive Lateral Injection", AIAA J., Vol. 13, No. 11, Nov. 1975, pp. 1441-1447

10. Vaglio Laurin, R., "On the PLK Method and the Supersonic Blunt Body Problem", Jour. Aerospace Sciences, Vol. 29, No. 2, Feb. 1962, pp. 185-206

11. Townsend, A.A., "The Behavior of a Turbulent Boundary Layer Near Separation", Jour. Fluid Mech., Vol. 12, No. 4, 1962, pp. 536-556

12. Widhopf, G.F. and Victoria, K. J., "Numerical Solution of the Unsteady Navier-Stokes Equations for the Oscillatory Flow Over a Concave Body", SAMSO TR No. 75-66, Sept. 1974.

13. Lax, P.D., "Weak Solutions of Nonlinear Hyperbolic Equations and Their Numerical Computation", Communications in Pure and Applied Mathematics, Vol. 7, Jan. 1954, pp. 159-193.

14. Lax, P.D. and Wendroff, B., "Systems of Conservation Laws", Communications in Pure and Applied Mathematics, Vol. 13, Feb. 1960, pp. 217-237.
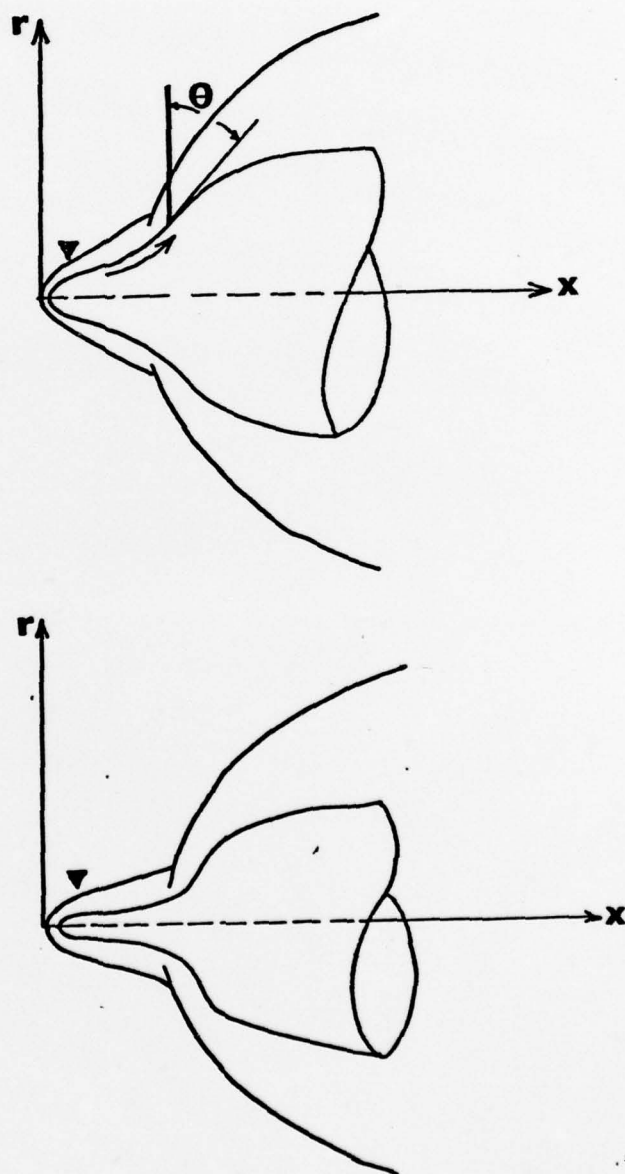
Figure 1. Schematic diagram of ablating nose-tip configurations: Sub-critical turbulent (top) and critical turbulent (bottom).▽denotes probable location of boundary layer transition.
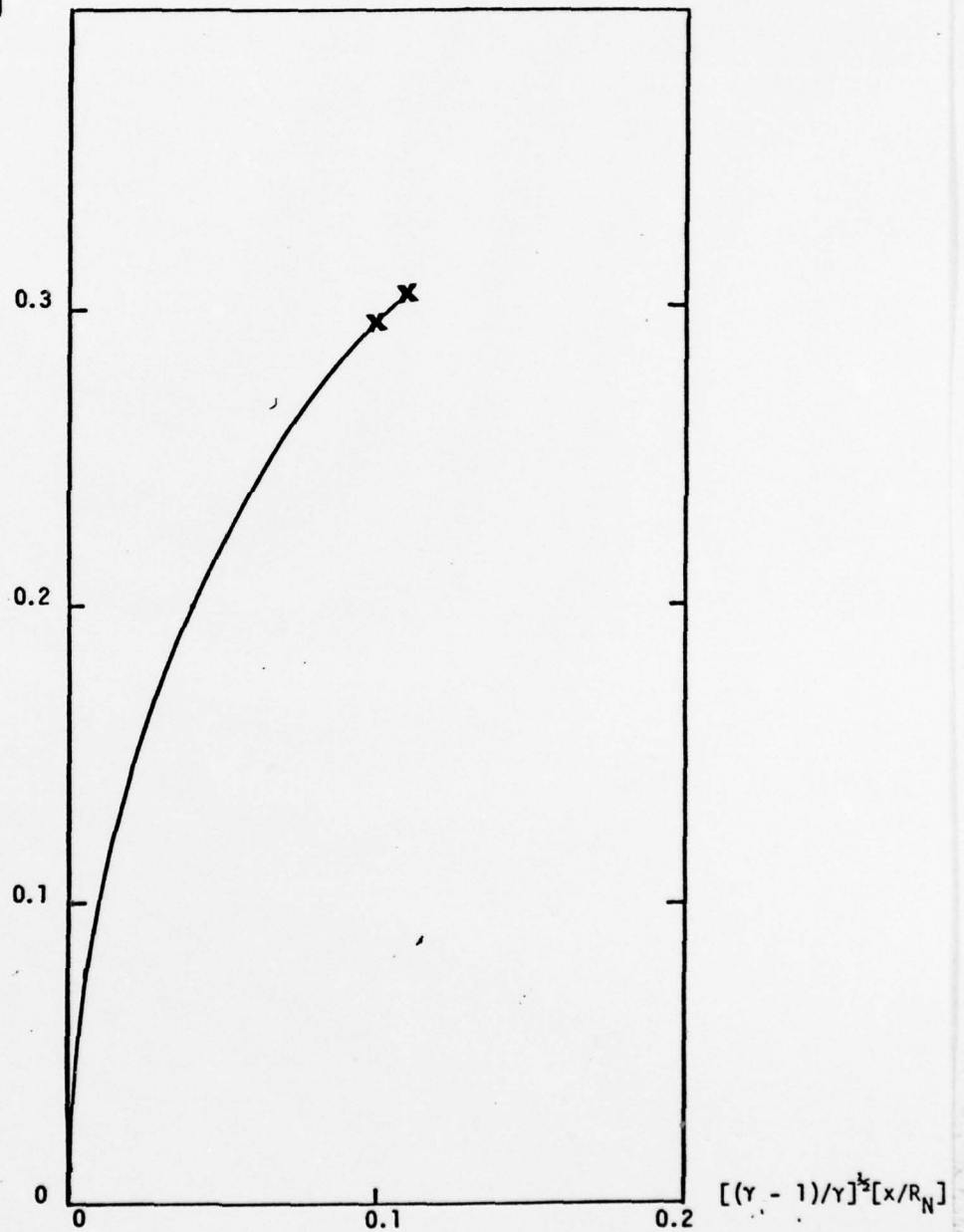
-22-

Figure 2. Calculated blunt self-preserving laminar shape, $\gamma = 7/5$. x denotes $\theta = \theta_\ell$; + denotes $\theta = \theta*$.

-23-

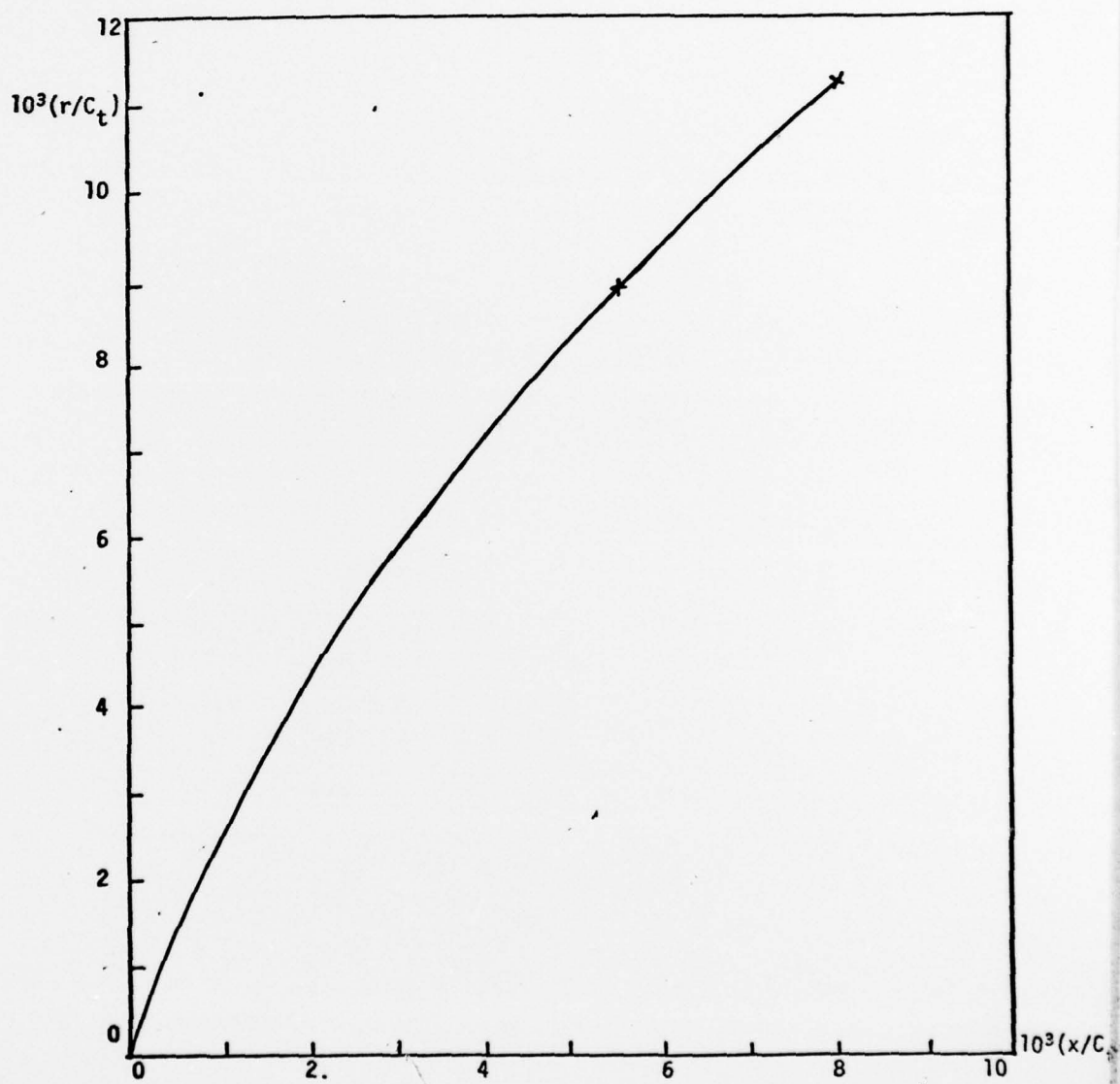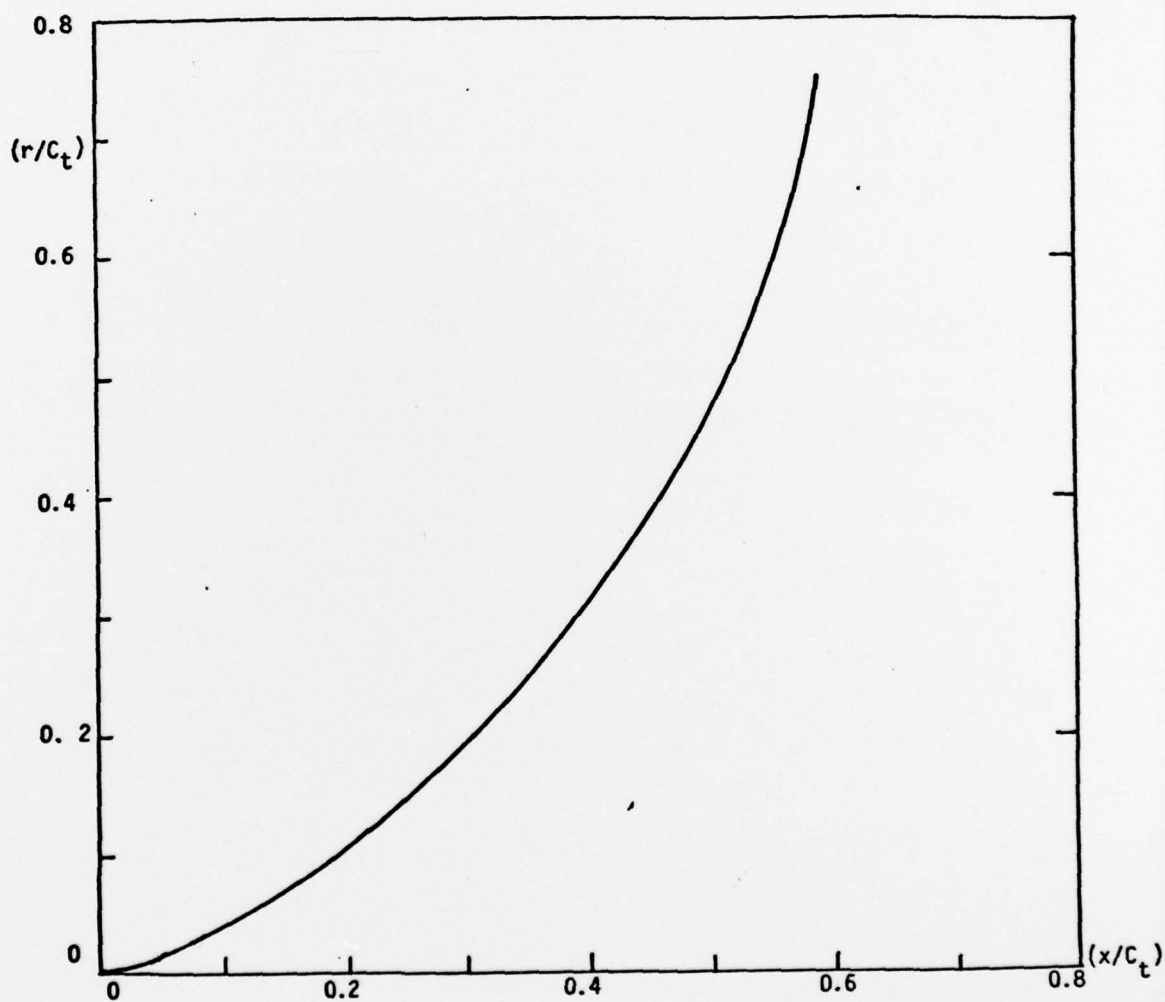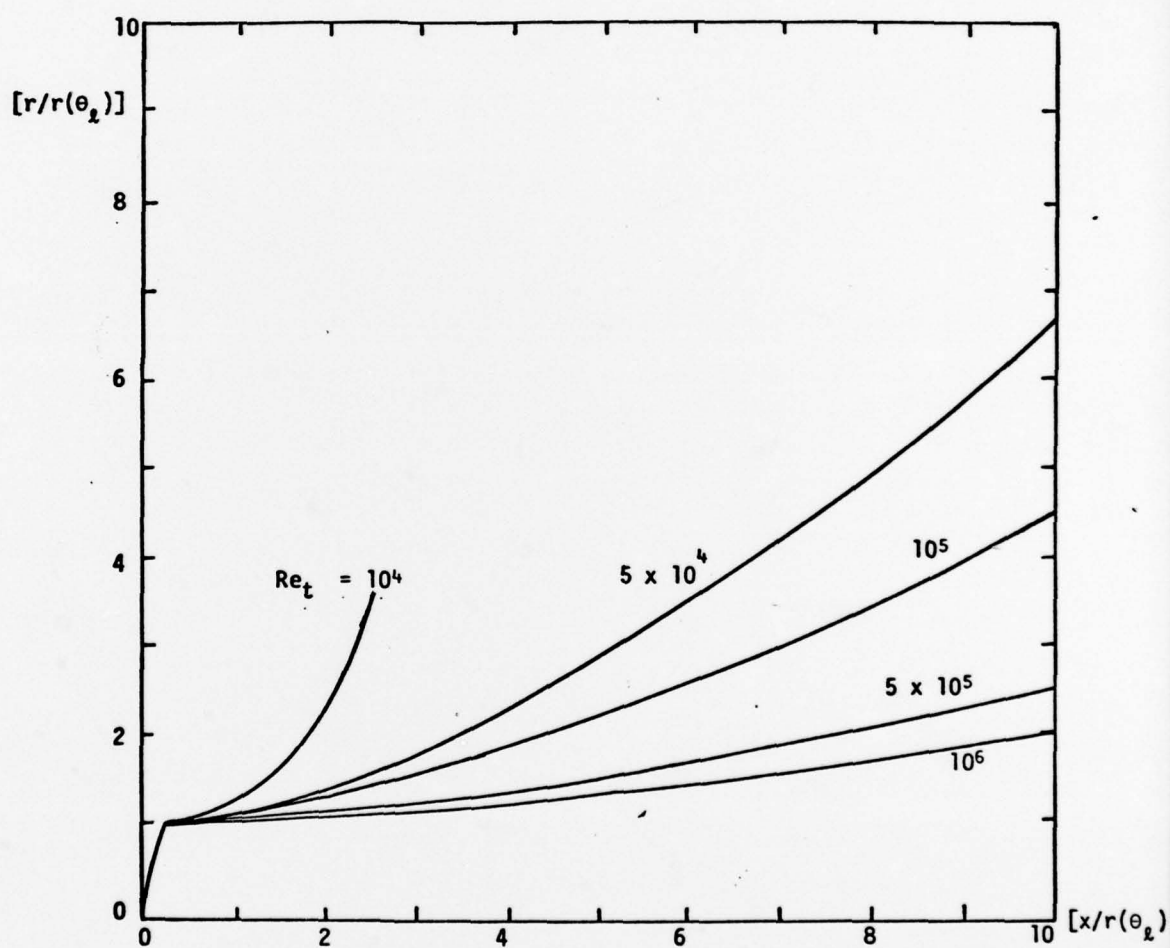Figure 3. Calculated blunt self-preserving turbulent shape, $\gamma \approx 7/5$.
x denotes $\theta = \theta_t$; + denotes $\theta = \theta^*$.

-24-

Figure 4. Calculated slender self-preserving turbulent shape.

Figure 5. Calculated matched blunt-laminar/slender-turbulent self-preserving shapes; $j = 1$, $\gamma = 7/5$.
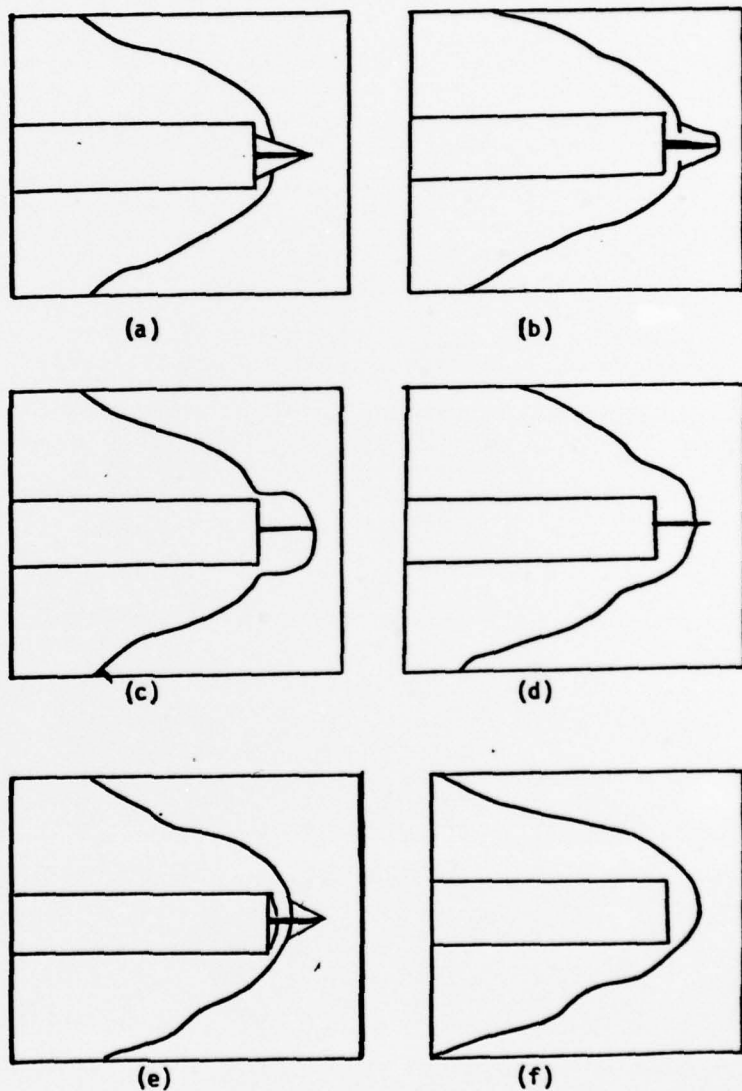
Figure 6. (a,b,c,d,e) Schematic diagrams of the oscillatory shock
pattern in the M_∞ = 6.8 flow over a spiked flat-headed
cylinder. (f) Shock pattern around a flat-header cylinder
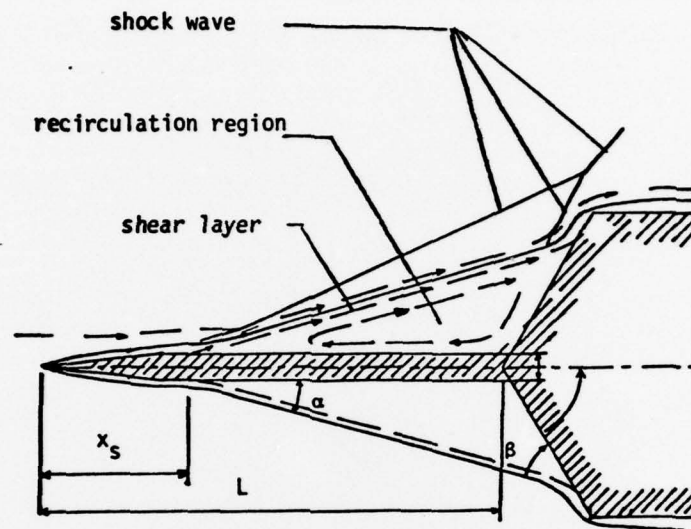with front air injection against the main stream.
After Reference 5.

shock wave

recirculation region

shear layer

x_s

α

β

L

compression

velocity profile

expansion

β

dividing streamline

(b)
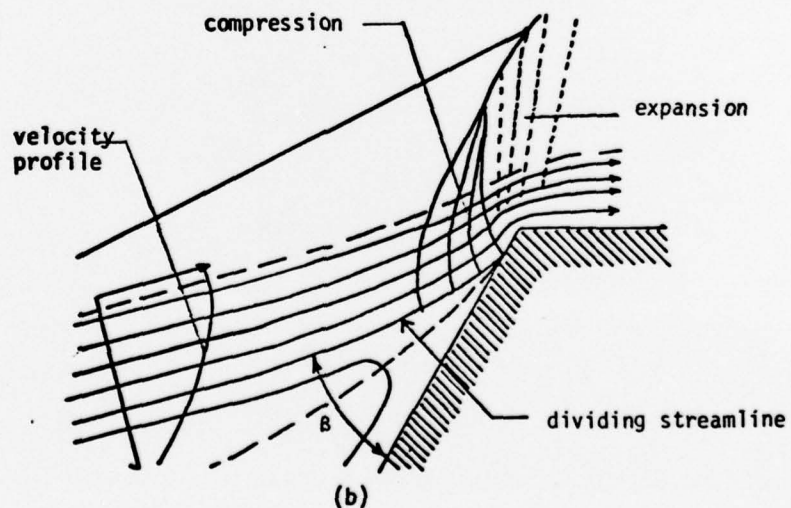
Figure 7. Schematic diagrams of flow pattern around spiked blunt body.
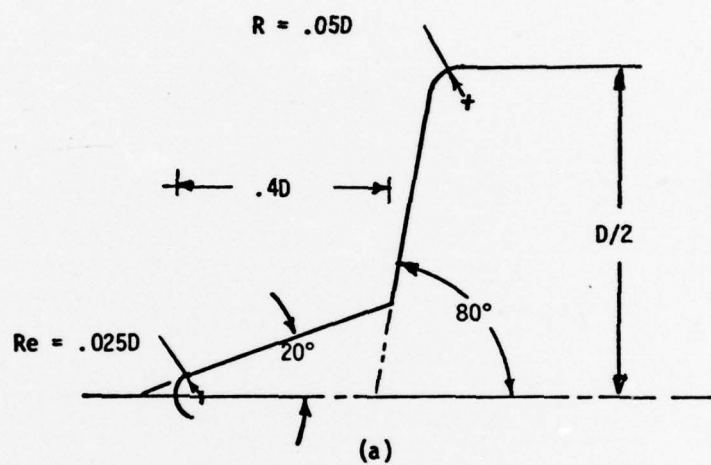(a) Overall. (b) Detail near reattachment point.
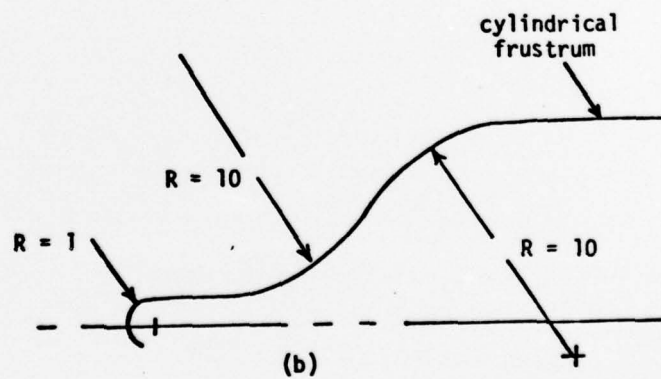
Figure 8. Geometry of nose tips investigated in Reference 8.
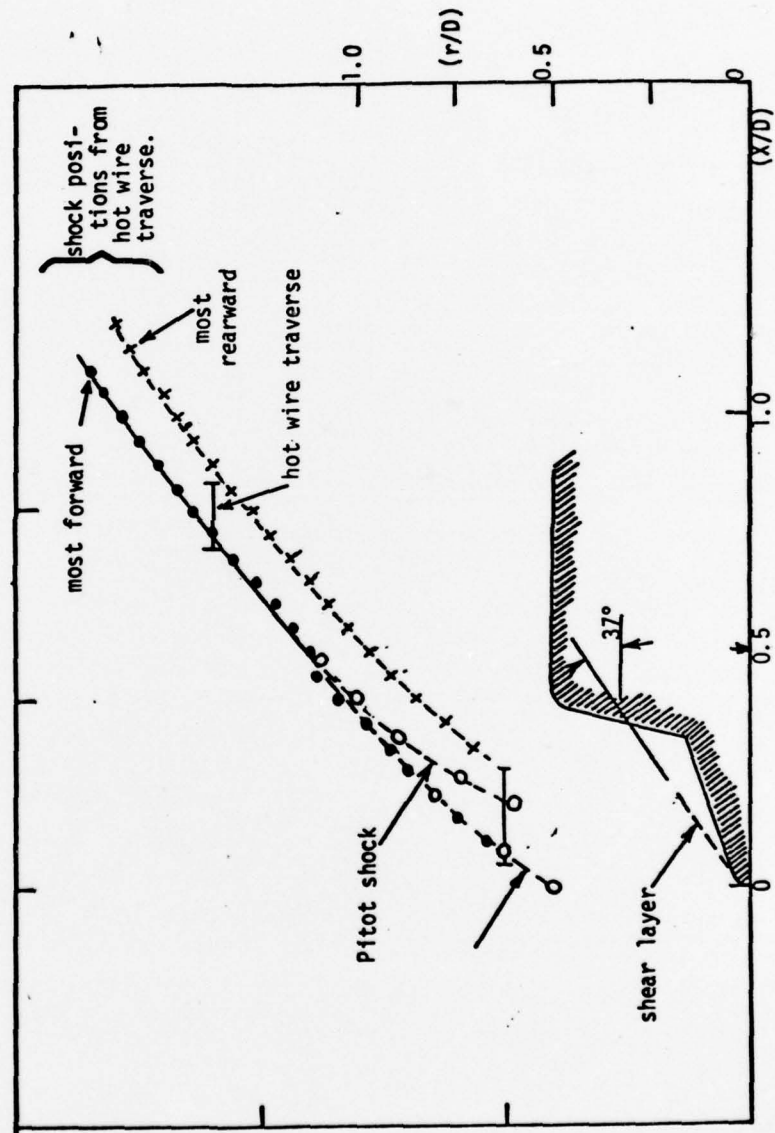(a) PANT-1, critical. (b) Proboscioid "1-10-10",
subcritical.

Figure 9. Map of the oscillating PANT-1 flow field observed in Reference 8.
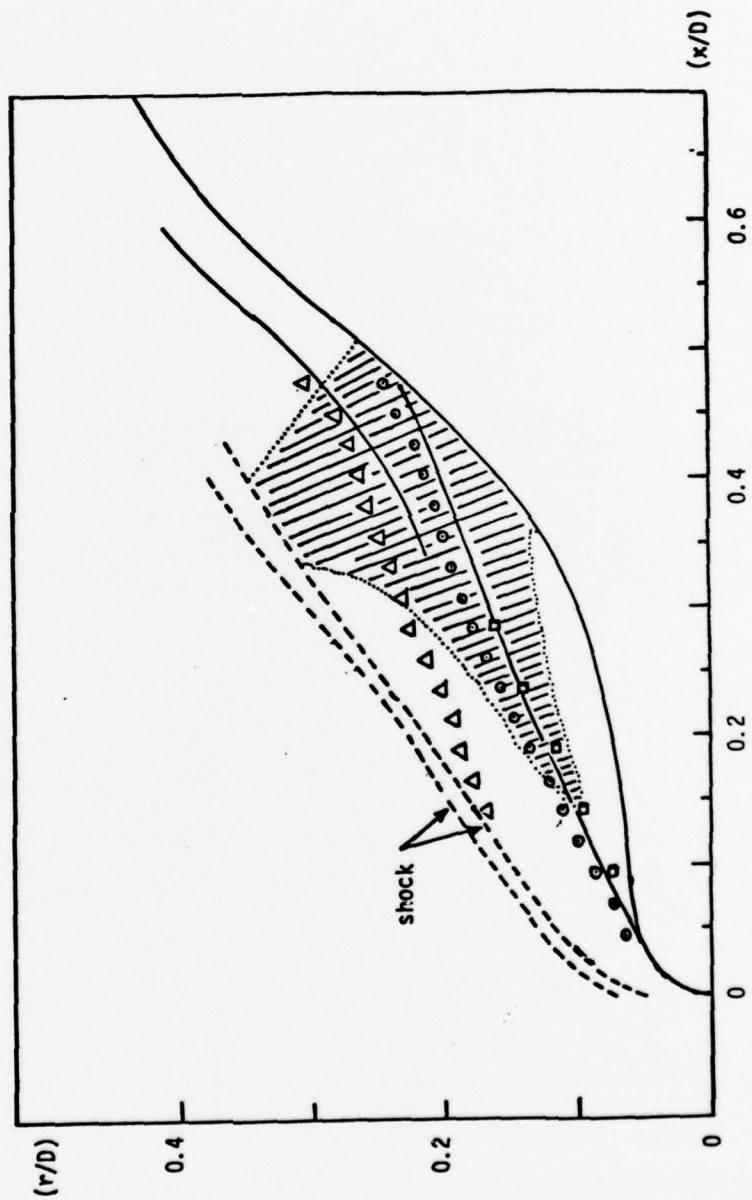
Figure 10. Map of the "1-10-10" flow field observed in Reference 8 at $Re_D = 1.5 \times 10^5$.

▨ Region exhibiting flow fluctuations.

——— , △ , o, ☐ Edges of shear layer observed with pitot tubes and hot wire.

REPORT DOCUMENTATION PAGE	READ INSTRUCTIONS BEFORE COMPLETING FORM

1. REPORT NUMBER AFOSR - TR - 77 - 0542	2. GOVT ACCESSION NO.	3. RECIPIENT'S CATALOG NUMBER

4. TITLE (and Subtitle) DEVELOPMENT AND AERODYNAMICS OF PROBOSCIOID ABLATING NOSE TIPS.	5. TYPE OF REPORT & PERIOD COVERED FINAL 1 May 1974 - 31 Oct 75
	6. PERFORMING ORG. REPORT NUMBER

7. AUTHOR(s) R. VAGLIO-LAURIN	8. CONTRACT OR GRANT NUMBER(s) F44620-74-C-0074

9. PERFORMING ORGANIZATION NAME AND ADDRESS NEW YORK UNIVERSITY DEPARTMENT OF APPLIED SCIENCES, NEW YORK, N.Y. 10003	10. PROGRAM ELEMENT, PROJECT, TASK AREA & WORK UNIT NUMBERS 9783-06 61102F

11. CONTROLLING OFFICE NAME AND ADDRESS AIR FORCE OFFICE OF SCIENTIFIC RESEARCH/NA BLDG 410 BOLLING AIR FORCE BASE, D C 20332	12. REPORT DATE March 1977
	13. NUMBER OF PAGES 33

14. MONITORING AGENCY NAME & ADDRESS(if different from Controlling Office)	15. SECURITY CLASS. (of this report) UNCLASSIFIED
	15a. DECLASSIFICATION/DOWNGRADING SCHEDULE

16. DISTRIBUTION STATEMENT (of this Report)

Approved for public release; distribution unlimited.

17. DISTRIBUTION STATEMENT (of the abstract entered in Block 20, if different from Report)

18. SUPPLEMENTARY NOTES

19. KEY WORDS (Continue on reverse side if necessary and identify by block number)

REENTRY HEATING
REENTRY AERODYNAMICS
ABLATION

409964

20. ABSTRACT (Continue on reverse side if necessary and identify by block number)

Rationalization of slender concave shapes on ablating nose tips is obtained in terms of composite laminar/turbulent self-preserving solutions to the nose recession problem. The occurrence of subcritical and critical (violently oscillatory) flow conditions is discussed and associated with specific geometrical characteristics of the ablating nose shape. The presence of distinct oscillatory modes is noted for both the subcritical and critical cases, and the distinct underlying inviscid instability mechanisms are pointed out. On that basis numerical flow analyses by extension of available unsteady inviscid flow models is suggested, and the nature of the required extensions is outlined.